npj | quantum materials

Article

Published in partnership with Nanjing University

https://doi.org/10.1038/s41535-024-00637-3

One-dimensional topological phase and tunable soliton states in atomic nanolines on Si(001) surface

Biyu Song[1,2], Guoxiang Zhi[2,3], Chenqiang Hua[2,3], Meimei Wu[2,3], Wenzhen Dou[1,2], Wenjin Gao[1,2], Tianzhao Li[1,2], Tianchao Niu[2,3] & Miao Zhou[1,2,3]

Formation of exotic topological states on technologically important semiconductor substrate is significant from the aspects of both fundamental research and practical implementation. Here, we demonstrate one-dimensional (1D) topological phase and tunable soliton states in atomic nanolines self-assembled on Si(001) surface. By first-principles calculations and tight-binding modeling, we reveal that Bi nanolines provide an ideal system to realize a multi-orbital Su–Schrieffer–Heeger (SSH) model, and the electronic properties can be modulated by *substrate-orbital-filtering* effect. The topological features are confirmed by nontrivial end states for a finite-length nanoline and (anti-)soliton states at the boundary of two topologically distinct phases. We demonstrate that solitons are highly mobile on the surface, and their formation could be controlled by surface B/N doping. As these nanolines can extend several micrometers long without kinks, and quantum transport simulations suggest clear signatures of topological states characterized by transmission resonance peaks, our work paves an avenue to achieve 1D topological phase compatible with semiconductor technology and to engineer the properties with high tunability and fidelity for quantum information processing.

The past decade has witnessed a massive surge of research interest in exploring exotic quantum states in solid-state materials. As an example, topological insulators (TIs), with metallic surface/edge states protected by time-reversal symmetry, have attracted tremendous attention in condensed matter physics and materials science communities with significant implications for dissipationless electronic transport and quantum computing applications[1–3]. While plenty of studies have focused on three-dimensional (3D)[4–6] or two-dimensional (2D)[7,8] TIs, one-dimensional (1D) topological systems have gained renewed interest recently. Compared to the conducting contour/surface states in 2D/3D counterparts, the unique features of 1D TIs lie in the localized topological states that provide promising platforms for robust information processing[9–11]. In 1D TIs, the Su–Schrieffer–Heeger (SSH) model[12–14] provides a paradigmatic model for searching materials, which describes a 1D dimerized lattice with two different alternating hopping strengths hosting topologically protected end modes and soliton excitations. Over the last years, a variety of 1D structures have been proposed to exhibit a topologically nontrivial phase, including polymer chains[12–15], indium nanowires[16–19], graphene nanoribbons[20–22], as well as engineered systems, such as ultracold atoms[23–25], acoustic lattices[26,27], electrical circuits[28] and photonic crystals[29–31].

One critical challenge to achieve 1D topological phase is the material availability. So far, successful detections of topological states in 1D electronic materials are rare[16,32–36]. On the one hand, the topologically localized states of 1D system such as polyacetylene are difficult to measure due to the weak structural stability[37]. On the other hand, low-dimensional structures normally need a certain substrate during synthesis or device setting, so that the electronic properties can be severely affected, as demonstrated in previously reported quantum spin Hall (QSH) insulators supported on semiconductor substrate[38,39]. Recently, coupled double indium chains[16] and silicon trimer chains[32] were grown on Si(111) and Si(553)-Au surface respectively, which exhibit intriguing phenomena such as chiral soliton excitations and trimer solitons. In this sense, formation of novel quantum phase on technologically important semiconductor substrate is of paramount significance, as it allows both facile manipulation of the topological states and intrinsic compatibility with current mature semiconductor technology.

Si(001) substrate lays the foundation for modern electronic devices, and construction of atomic quantum wires on the surface has been broadly explored in literature[40–43]. Here, we focus on Bi, which has been used as a surfactant (as an alternative to As or Sb) during Si or Ge growth on Si(001) or Ge(001)[40–43]. Deposition of Bi on Si(001) forms straight nanolines

[1]School of Physics, Beihang University, Beijing 100191, China. [2]International Innovation Institute, Beihang University, Hangzhou 311115, China. [3]Tianmushan Laboratory, Hangzhou 310023, China. e-mail: mzhou@buaa.edu.cn

consisting of two rows of Bi dimers. These nanolines are striking in uniformity, which appear only 1.5 nm in width but extend to ~400 nm without kinks. The geometry and microscopic formation mechanism have been discussed in detail[44–46]. Generally, there are two accepted structural models for Bi nanolines on Si(001), with Miki model[41] composed by a pair of self-assembled Bi dimer chains separated by a missing Si dimer defect (see Fig. 1a, c), and Haiku model[42] involving reconstructed subsurface layers of Si underneath Bi dimers (Fig. 1b, d). Interestingly, the alternating bond length of Bi chains resembles that of polyacetylene, so that 1D topological phase may appear according to the SSH model[12–14].

In this work, by combining density functional theory (DFT) based first-principles calculations and tight-binding (TB) modeling, we demonstrate 1D topological phase and tunable soliton states in Bi nanolines self-assembled on Si(001) substrate [Bi/Si(001)]. Spontaneous dimerization of Bi opens a topological gap at the boundary of Brillouin zone, so that nontrivial localized modes arise at the two ends of finite-size nanolines. We develop a multi-orbital SSH model and reveal that the electronic structures of Bi/Si(001) can be effectively regulated by *substrate-orbital-filtering* effect[38,39]. Remarkably, topological soliton states can be realized by joining two topologically distinct phases. These solitons are highly mobile on the surface, and their stability is controllable by surface B/N doping. Through quantum transport calculations, we suggest the observation of topological states by transmission resonance peaks as clear signatures in practical experiment. These results should stimulate immediate experimental interest in characterizing 1D topological states in available systems, thus providing an attractive platform to manipulate exotic quantum states compatible with semiconductor technology for future applications.

Results

Electronic structures

Figure 1 shows the optimized structures of Bi/Si(001) with Miki[41] and Haiku[42] models, where a pair of parallel Bi chains are formed on a hydrogenated $p(2\times2)$-reconstructed Si(001) surface. Both structures contain Bi dimer pairs at the topmost layer extending along [110] crystallographic direction of the surface into arrays. The main difference between the two models lies in the reconstruction of subsurface layers, where only Haiku type exhibits reconstructed 5-7-5 membered Si rings below the grown Bi. As a result, the inter-chain distances are 6.69 and 6.37 Å for Miki and Haiku models, respectively. We also simulated the scanning tunneling microscopy (STM) images, which show clear Peierls distortions of Bi atoms to form dimers, matching well with experimental observations[43]. Such structural distortions suggest a charge density wave state driven by the 1D metallic band of Bi atoms, as we shall see later.

We then explored the electronic properties by calculating the band structures. To understand the influence of Bi dimerization, we first considered artificial structures with equally spaced Bi atoms (without Peierls distortion) on Si(001) surface (see Supplementary Fig. 1). As shown in Fig. 2, for both Miki and Haiku models without Bi dimerization, two pairs of linearly dispersed bands can be observed within the bulk gap of Si, which cross each other and form Dirac points at the boundary of Brillouin zone (Y point) near Fermi level (Fig. 2a, c). Analyses on band composition reveal that the Dirac bands are mainly contributed by the p_y orbitals of Bi atoms. However, the equally spaced Bi atoms are unstable and spontaneously relax to the dimerized configurations (Fig. 1). We found that Bi dimerization splits the Dirac points with a large band gap. Specifically, for Miki model (Fig. 2b), an energy gap of 1.46 eV is formed at Y point, while the global gap has a value of 1.23 eV due to the presence of Si bulk states. Similarly, for Haiku model (Fig. 2d), a large gap of 1.55 eV is obtained at Y and the global gap is 1.02 eV. The appearance of two pairs of Dirac bands could be understood by the fact that there are two parallel Bi chains within one nanoline, so that four Bi atoms are present in each unit cell.

We also calculated the partial density of states (DOS) of the two systems, as presented in Supplementary Fig. 2. It was found that the p_x and p_z orbitals of Bi hybridize strongly with the electronic states of Si, while the remaining p_y orbital forms Dirac bands within the Si bulk gap. This clearly reflects the *substrate-orbital-filtering* effect that ensures both high structural

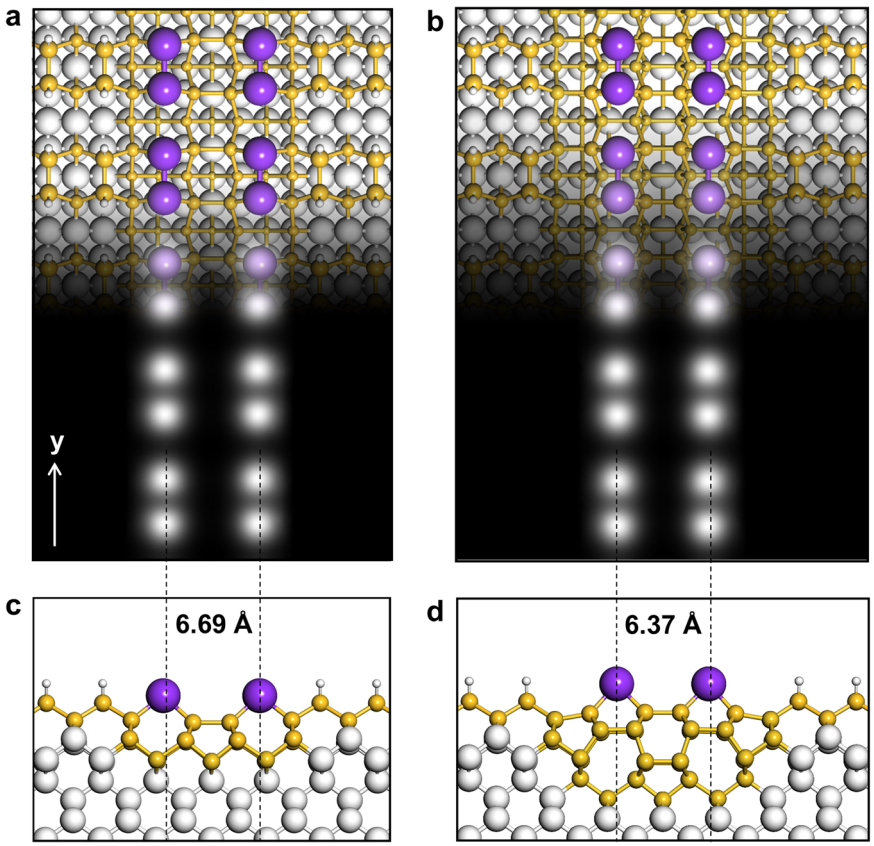

Fig. 1 | Optimized structures of Bi/Si(001). Top and side views of Miki model (**a**, **c**) and Haiku model (**b**, **d**). Big purple and small white balls represent Bi and H atoms, respectively. Big white balls denote Si atoms, where the atoms around Bi are shown in yellow, highlighting the structural reconstruction. The simulated STM images are also included.

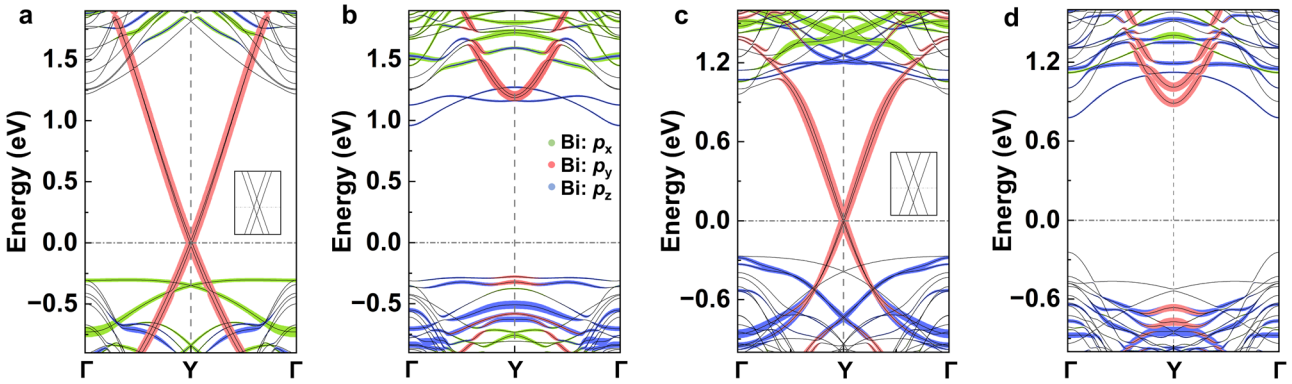

Fig. 2 | Band structures of Bi/Si(001) without and with Bi dimerization. a, **b** Miki model and (**c**, **d**) Haiku model, where the contributions from p_x, p_y and p_z orbitals of Bi are highlighted. Fermi level is set to zero.

stability and intriguing band properties[38,39]. Inclusion of spin-orbit coupling (SOC) lifts the spin degeneracy and results in Rashba-split bands (Supplementary Fig. 3). Furthermore, as standard DFT usually underestimates the band gap of semiconductors, we also checked the results by the more sophisticated hybrid functional (HSE06)[47,48], which show similar band structures but with larger energy gaps (Supplementary Fig. 4).

The topological properties of Bi nanolines can be characterized by the so-called Zak phase (φ_{Zak})[49], which is derived from the integral of Berry connection over Brillouin zone,

$$\varphi_{Zak} = \sum_n \gamma_n = \sum_n i \int_{-\pi/a}^{\pi/a} \langle u_{nk} | \partial_k | u_{nk} \rangle dk, \quad (1)$$

where γ_n is the Zak phase for the nth band, $|u_{nk}\rangle$ is the periodic part of Bloch function for the nth band at the momentum k, and the summation is over all occupied bands. Due to the strong hybridization of p_x and p_z orbitals of Bi with the electronic states of Si substrate, the disentanglement is rather difficult. Fortunately, as the Dirac bands contributed by Bi p_y orbital are mostly located inside the bulk gap of Si, we can disentangle this orbital from others and obtain the Wannier function by projecting the DFT wavefunction onto the Bi p_y orbital (see Supplementary Fig. 5), so that the Zak phase can be calculated. Results show that when the intercell hopping of Bi p_y is larger than the intracell hopping, $\varphi_{Zak} = \pi$ for a Bi chain on the substrate, indicating a topologically nontrivial phase; whereas when the intracell hopping is larger, the chain is topologically trivial with $\varphi_{Zak} = 0$. More results on the topological characteristics are presented in Supplementary Information Note 1, confirming the topological feature. Therefore, depending on the choice of unit cell, Bi nanolines can exist in two topologically distinct phases that is protected by mirror symmetry, and for the nontrivial phase, topological edge states should appear when an open boundary condition is applied.

To directly characterize the topological features of Bi/Si(001), we constructed Bi nanolines of finite size on the surface for the two distinct phases. As shown in the insets of Fig. 3, phase A has perfect Bi dimers at the two ends of nanolines, while there are missing Bi atoms at the two ends in phase B. Such systems could be achieved by using an STM tip-assisted manipulation technique[50–52]: With atomic-level control, one can obtain phase B by removing one Bi atom from the dimer at two ends. After structural optimization, the systems remain stable. We then calculated the discrete energy levels of finite-size Bi nanolines for the two phases. Figure 3a–d presents the energy levels on Bi nanolines with a length of 6 times the unit cell, and results on longer nanolines are shown in Supplementary Fig. 6. Clearly, for both Miki and Haiku models, phase A has no end modes within the bulk gap (Fig. 3a, c), suggesting a topologically trivial phase. In contrast, topological end modes emerge in the topological gap of phase B (Fig. 3b, d), thus turning the systems into a topologically nontrivial phase. Furthermore, we plot out the real-space charge density distributions of the topological end states and bulk states for phase B. As shown in Fig. 3e–h, there are two pairs of electronic states that are mainly spread over the four ends of Bi nanolines (Fig. 3e, g), thus contributing to the four localized end states, which are characterized by a π Zak phase. The bulk states, however, are distributed over the central region (Fig. 3f, h). The topological end states can also be identified by partial DOS (Supplementary Fig. 7), where a sharp peak is present near Fermi level for the topologically nontrivial phase, ideal for scanning tunneling spectroscopy (STS)[16] characterization.

Multi-orbital SSH Model

The physical origin of 1D topological phase in Bi/Si(001) is attributed to the dimerized structure, which can be explained by the SSH model[12–14]. However, as the valence electrons of Bi involve p_x, p_y and p_z orbitals, we need to construct a multi-orbital SSH Hamiltonian with (p_x, p_y, p_z) orbitals. We first considered a single Bi dimer chain (Fig. 4a), for which the Hamiltonian is expressed as,

$$H = \sum_{ijmn} (t_{mn} c^{\dagger}_{A_{im}} c_{B_{jn}} \delta_{ij} + t'_{mn} c^{\dagger}_{B_{im}} c_{A_{jn}} \delta_{i,j-1}) + h.c. \quad (2)$$

where $c^{\dagger}_{Aim}(c_{Bjn})$ is the creation (annihilation) operator for the $m(n)$-th orbital of A(B) atom in the $i(j)$-th unit cell and $t_{mn}(t'_{mn})$ represents the intracell (intercell) hopping strength. Only the nearest-neighbor interactions were included here. Diagonalization of Eq. (2) gives six bands for an infinite Bi chain. Without Bi dimerization ($t_{mm} = t'_{mn}$), there are three Dirac bands forming Dirac points at the boundary (Y point) of Brillouin zone (Fig. 4b). The bands contributed by p_x and p_z orbitals are degenerate due to the rotational symmetry of structure. With dimerization ($t_{mm} \neq t'_{mn}$), the Dirac points are split (Fig. 4c). The gap can be topologically trivial ($t_{mm} > t'_{mn}$) or nontrivial ($t_{mm} < t'_{mn}$), as confirmed by calculating the discrete energy levels of a finite-length chain. Specifically, for the nontrivial phase (phase B), there are three pairs of degenerate topological end modes localized within the bulk gap, as contributed by three (p_x, p_y, p_z) orbitals. Considering the possible *substrate-orbital-filtering* effect as observed in Bi/Si(001), we explored the cases with two orbitals (p_x, p_y) and a single orbital (p_y) on each site. It was found that the (p_x, p_y)-orbital Hamiltonian produces four Dirac bands and two pairs of degenerate end modes (Fig. 4e–g), while the single-orbital Hamiltonian generates two Dirac bands and two end modes within the bulk gap (Fig. 4h–j), in accordance with the original SSH model[12–14].

As there are two parallel chains within one Bi nanoline, we then constructed the Hamiltonian with two Bi chains by applying an interaction

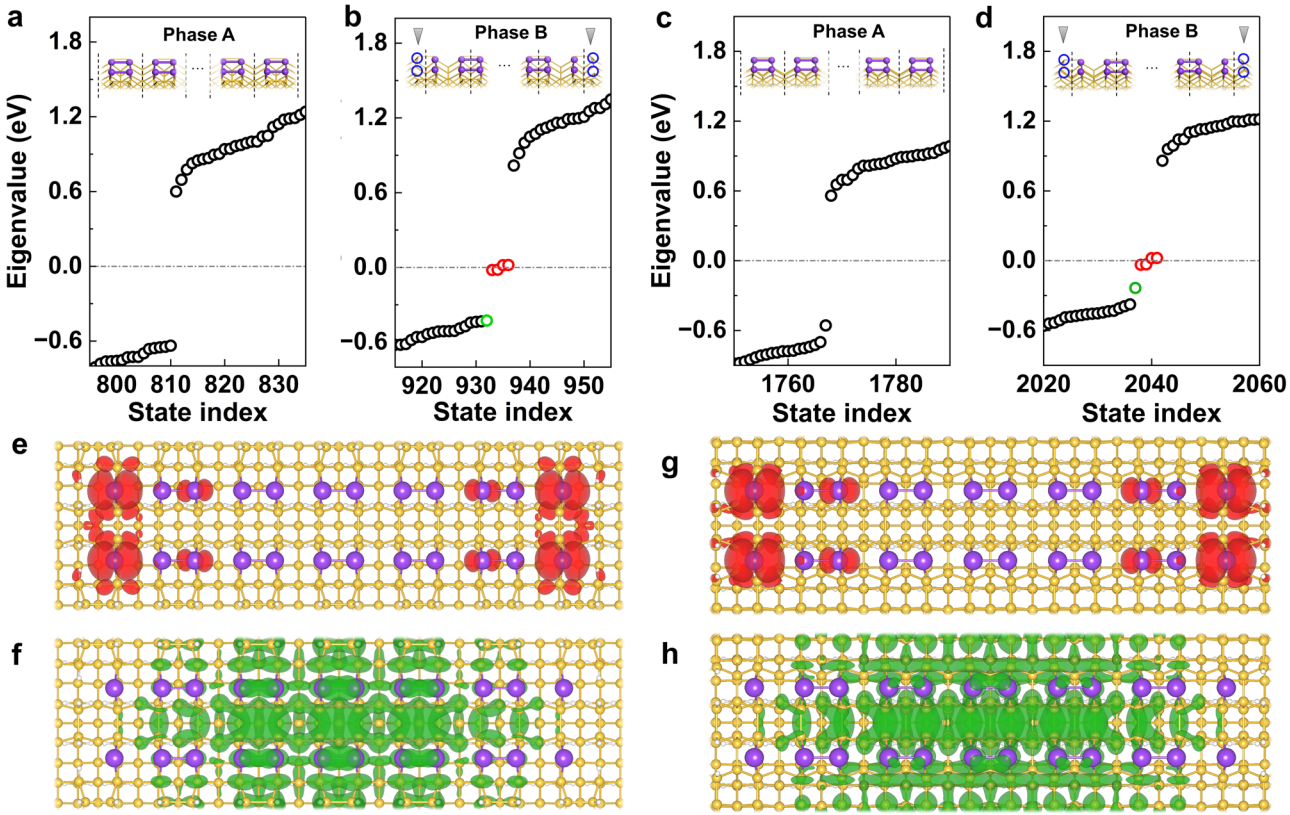

Fig. 3 | Calculated discrete energy levels and charge density distributions of finite-size Bi nanolines on Si(001). a, **b** Miki model and (**c**, **d**) Haiku model, where the topological end states are denoted by red circles and bulk states by black circles. Creation of phase A and phase B is illustrated in the insets, with the unit cell indicated by black dotted lines. Spatial distributions of charge density for Miki model (**e**, **f**) and Haiku model (**g**, **h**). The topological end states are shown in red and bulk states in green (Isovalue = 5×10^{-4} e/Å^3).

term (η) describing the ladder inter-chain hopping (Fig. 4a). Within a single-orbital model, the reciprocal-space Hamiltonian is written as,

$$H = \begin{pmatrix} 0 & t + t'^{\dagger} e^{-ik} & \eta & 0 \\ t^{\dagger} + t' e^{ik} & 0 & 0 & \eta \\ \eta^{\dagger} & 0 & 0 & t + t'^{\dagger} e^{-ik} \\ 0 & \eta^{\dagger} & t^{\dagger} + t' e^{ik} & 0 \end{pmatrix} \quad (3)$$

Results show that the parallel double chains exhibit two pairs of Dirac bands (Fig. 4k), and the energy of band splitting between the two pairs is proportional to η. Bi dimerization splits the Dirac points (Fig. 4l), and two pairs of localized edge modes appear (Fig. 4m) due to the existence of four ends within two finite-size chains. It should be noted that there are two different ground-state phases when two dimerized chains are combined, which can be denoted as AA and AB (Supplementary Fig. 8), and Bi/Si(001) corresponds to the AA phase. Interestingly, by fitting the TB band structures with DFT results, we can extract the value of η, being 0.04 and 0.1 eV for Miki and Haiku model, respectively. This is in perfect agreement with the fact that Haiku model has longer inter-chain distance (6.69 Å) than Haiku (6.37 Å).

Soliton states

For 1D topological system, soliton states can emerge at the boundary of two topologically distinct phases. This could be achieved by introducing structural defects intentionally or unintentionally in experiments[32]. Here, we considered two types of defect at the boundary between phase A and phase B, one with two long (weak) Bi-Bi bonds and the other with two short (strong) Bi-Bi bonds. There are two domain walls in each Bi chain within the constructed nanolines, where periodic boundary condition is applied. The calculated discrete energy levels and charge density distributions for Miki model are presented in Fig. 5 and Haiku model in Supplementary Fig. 9. It was found that the structure with long Bi-Bi bonds at the boundary exhibits two pairs of domain wall states (Fig. 5a). These states are spread over the domain wall region with a mirror symmetry (Fig. 5b), which are filling anomalous[53,54]. Similarly, two pairs of domain wall states were also observed for the structure with short Bi-Bi bonds at the boundary (Fig. 5c, d). By analyzing the vanishing behaviors of these states on even or odd sites of the lattice[14], we can assign the two defects as solitons and anti-solitons, respectively. Importantly, for both solitons and anti-solitons, the spatial distribution decays away from the domain wall and can extend several unit cells, in sharp contrast to conventional defects (vacancies, adatoms, etc.) that are strongly localized. This could be facilely distinguished by STM imaging[32,46].

For potential applications of the localized topological states, such as in quantum information transfer and processing, it is essential to have solitons that are mobile[32]. We then explored the stability and energetic properties of (anti-)solitons in Bi/Si(001). It was found that energy of the structure with solitons (Fig. 5b) is ~0.05 eV higher than that with anti-solitons (Fig. 5d), so we focused on the anti-solitons. By using the climbing-image nudged elastic band method[55], we evaluated the propagation barrier of an anti-soliton moving along a Bi nanoline (see Supplementary Fig. 10). The obtained barrier is ~0.02 eV, indicating high mobility on the surface. Furthermore, we calculated the formation energy, as defined by, $E_f = (E_a\text{-}E_p)/n$, where E_a and E_p represent the total energies of the system with and without anti-solitons respectively, and n is the number of anti-solitons. It was found that the anti-soliton has a formation energy of 0.69 eV (Miki model), suggesting an endothermal formation process.

We also noticed that the localized domain wall states induced by (anti-) solitons are half-occupied (Fig. 5a, c). Hence, by introducing electrons or

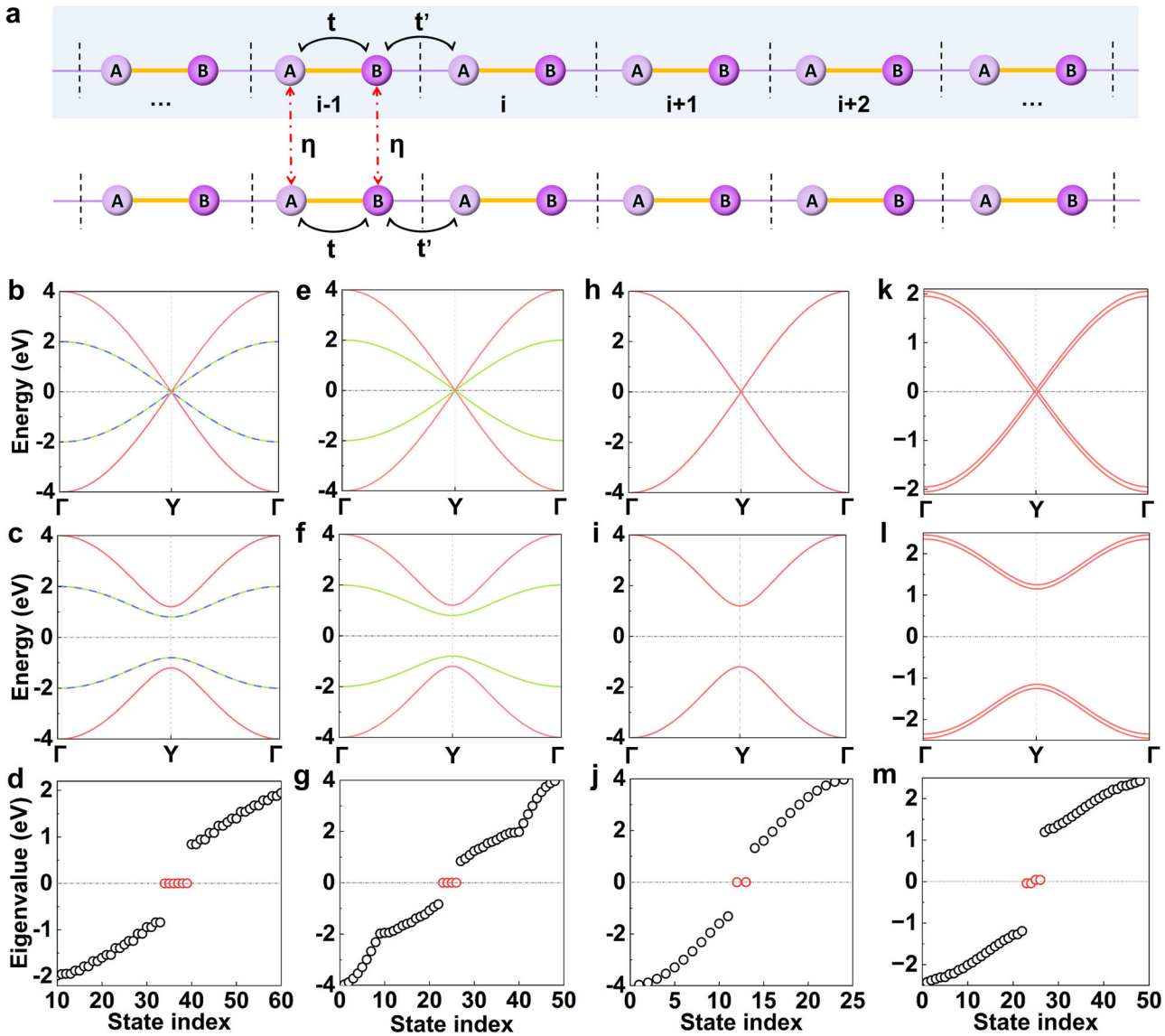

Fig. 4 | TB model and the calculated electronic structures for a Bi nanoline. **a** Schematic of the TB model. *i* denotes the index of unit cell with sublattice A/B. **b**–**d** Calculated band structures for a single Bi chain involving (p_x, p_y, p_z) orbitals without (**b**) Bi dimerization ($t = t'$=2.0 eV), with (**c**) Bi dimerization (t = 2.0 eV, t'-t = ±0.6 eV), and (**d**) discrete energy levels for the topological phase (t = 2.0 eV, t'-t = 0.6 eV). The green, red and blue curves represent the bands contributed by p_x, p_y and p_z orbitals, respectively. **e**–**g**, **h**–**j** Same as (**b**–**d**) for the cases involving (p_x, p_y) orbitals and a single p_y orbital, respectively. **k**–**m** Calculated band structures for a Bi nanoline with double chains involving a single p_y orbital without (**k**) Bi dimerization, with (**l**) Bi dimerization, and (**m**) discrete energy levels. The inter-chain interaction η is set to 0.04 eV.

holes at the conduction band minimum (CBM) or valance band maximum (VBM), transition from CBM to zero-energy states or from zero-energy states to VBM will occur with an energy release, so that the formation energy of (anti-)solitons may be reduced. In practice, this could be achieved by B or N doping in the Si substrate. Indeed, our calculations show that by B (N) doping, the formation energy of an anti-soliton is reduced to 0.23 (0.41) eV, much smaller than the case without doping (0.69 eV). The discrete energy levels and spatial distributions for the doped systems are presented in Fig. 5e–h, where empty (fully-filled) localized states can be observed, corresponding to positively (negatively) charged anti-solitons. We further calculated the occupation of anti-soliton states for pristine and B/N-doped Bi/Si(001), and the results are presented in Supplementary Table 1. It was revealed that the anti-solitons in pristine Bi/Si(001) are neutral with spin 1/2, and the anti-solitons in B/N-doped system are positively/negatively charged with spin zero (Supplementary Fig. 11). This behavior is peculiar, and can be described by spin-charge separation[14,53] The above analyses can also be applied to Haiku model (see Supplementary Table 2 and Supplementary Fig. 9), demonstrating the potential of chemical doping in regulating the physical properties of (anti-)solitons.

In practical experiments, individual solitons can be generated and annihilated at desired locations through the application of a voltage pulse from a STM tip[32]. For Bi/Si(001), the similar procedure could be employed. Meanwhile, the structures of (anti-)solitons could be atomically resolved by non-contact atomic force microscopy (AFM) imaging[32], and the physical properties could be characterized by STM/STS measurements[16,50–52]. As Bi nanolines can extend several micrometers long without kinks[43], and the created (anti-)solitons are highly mobile and tunable on the surface, the proposed structure thus provides an ideal system for experimental synthesis, characterization and control of localized topological states for potential applications.

Quantum transport

We constructed an electronic device by placing planar source and drain leads on Bi/Si(001) to simulate the experimental device setup, which is

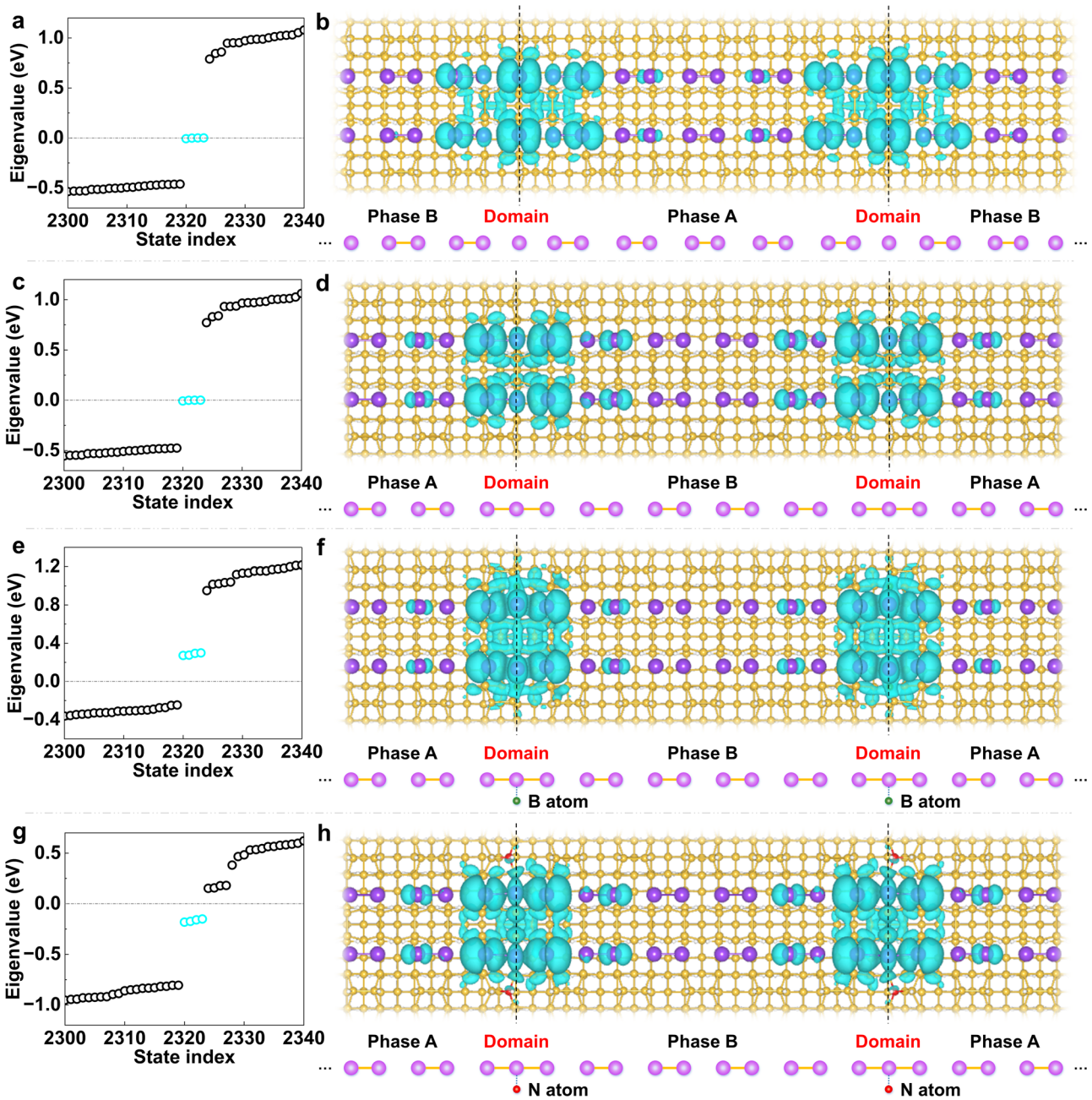

Fig. 5 | Creation of soliton and anti-soliton states in Bi/Si(001) with Miki model. **a**, **b** Calculated discrete energy levels and spatial charge distribution of solitons, where soliton states are highlighted by blue circles. **c**, **d** Energy levels and spatial charge distribution of anti-solitons. **e**, **f** B doping and (**g**, **h**) N doping effects on the electronic structures with anti-solitons

shown in Supplementary Fig. 12a. Quantum transport properties could be computed by the wave-guide theory and transfer-matrix method[56] (see details in Supplementary Information Note 2). We found that the number of transmission resonance peaks provides clear signatures of the topological phase: For a single Bi chain, two nearly degenerate peaks can be observed in the vicinity of zero energy (Supplementary Fig. 12b), corresponding to the two topological end states of one chain; for a Bi nanoline containing two chains, there are two pairs of nearly degenerate peaks, associated with the four nontrivial end states of two chains (Supplementary Fig. 12c). The small splitting between the two pairs of peaks originates from the weak inter-chain interaction. With increased (decreased) inter-chain coupling, the splitting will become larger (smaller), suggesting the capability of strain engineering in tuning the transport properties. In light of the mature strained Si technology, it is particularly attractive to manipulate the surface transport for versatile electronic/spintronic devices[57,58].

Discussion

In summary, we have demonstrated 1D topological phase and tunable (anti)-soliton states in atomic nanolines self-assembled on Si(001) substrate. The topological nature is confirmed by the existence of nontrivial end modes in finite-length nanolines and (anti-)soliton states at the boundary of two topologically distinct phases. A multi-orbital SSH model is developed to describe the electronic structures of Bi nanolines, which can be effectively modulated by the underlying Si(001) through *substrate-orbital-filtering* effect. Interestingly, (anti-) solitons are highly mobile on the surface, and the formation is readily controlled by chemical doping. We highlight the experimental

characterization of topological states by transport measurement with clear signatures of transmission resonance peaks. While this work focuses on Bi, the findings are expected to be generally applicable to other atomic nanolines on semiconductor substrates, such as Pt, Sn and Pb with similar dimerized structures[59–62]. Our results not only provide practical platforms to achieve 1D topological states compatible with semiconductor technology, but also show promise for using STM manipulation and strain engineering to further our ability to control exotic quantum states for quantum information applications.

Methods

First-principles calculations

First-principles calculations were performed within the framework of DFT using the projected augmented wave (PAW)[63,64] as implemented in the Vienna Ab initio Simulation Package (VASP) code[65,66]. The generalized gradient approximation (GGA) in Perdew-Burke-Ernzerhof (PBE)[67] format was used to describe the exchange-correlation functional. A cutoff energy of 400 eV was used for the plane wave basis set. Si(001) surface was modeled by a slab structure of seven atomic layers, and the bottom surface was terminated by H atoms in a dihydride structure. A $2 \times 8 \times 1$ Γ-centered k-point mesh was used to sample the Brillouin zone. During structural optimization, the lower two layers of Si and H atoms were fixed, while all other atoms were fully relaxed until the atomic forces were smaller than 0.01 eV/Å. A vacuum region of 20 Å was used to eliminate the interaction between neighboring slabs. Zak phase was calculated by WannierTools[68] based on the symmetrized real-space Wannier Hamiltonian obtained by Wannier90[69] and WannSymm code[70].

Data availability

Data are available from the corresponding author upon reasonable request.

Code availability

Code is available from the corresponding author upon reasonable request.

Received: 25 October 2023; Accepted: 28 February 2024;
Published online: 09 March 2024

References

1. Hasan, M. Z. & Kane, C. L. Colloquium: Topological insulators. *Rev. Mod. Phys.* **82**, 3045 (2010).
2. Qi, X. L. & Zhang, S. C. Topological insulators and superconductors. *Rev. Mod. Phys.* **83**, 1057 (2011).
3. Bradlyn, B. et al. Topological quantum chemistry. *Nature* **547**, 298–305 (2017).
4. Hsieh, D. et al. A topological Dirac insulator in a quantum spin hall phase. *Nature* **452**, 970–974 (2008).
5. Teo, J. C. Y., Fu, L. & Kane, C. L. Surface states and topological invariants in three-dimensional topological insulators. *Phys. Rev. B* **78**, 045426 (2008).
6. Nishide, A. et al. Direct mapping of the spin-filtered surface bands of a three-dimensional quantum spin hall insulators. *Phys. Rev. B* **81**, 041309 (2010).
7. Bernevig, B. A., Hughes, T. L. & Zhang, S. Quantum spin hall effect and Topological Phase transition in HgTe quantum wells. *Science* **314**, 1757–1761 (2006).
8. Wu, C., Bernevig, B. A. & Zhang, S. C. Helical liquid and the edge of quantum spin hall systems. *Phys. Rev. Lett.* **96**, 106401 (2006).
9. Guo, H. M. A brief review on one-dimensional topological insulators and superconductors. *Sci. China Phys. Mech. Astron.* **59**, 637401 (2016).
10. Mourik, V. et al. Signatures of majorana fermions in hybrid superconductor-semiconductor nanowire devices. *Science* **336**, 1003–1007 (2012).
11. Szumniak, P., Pawłowski, J., Bednarek, S. & Loss, D. Long-distance entanglement of soliton spin qubits in gated nanowires. *Phys. Rev. B* **92**, 035403 (2015).
12. Su, W. P., Schrieffer, J. R. & Heeger, A. J. Solitons in polyacetylene. *Phys. Rev. Lett.* **42**, 1689 (1979).
13. Su, W. P., Schrieffer, J. R. & Heeger, A. J. Soliton excitations in polyacetylene. *Phys. Rev. B* **22**, 2099 (1980).
14. Heeger, A. J., Kivelson, S., Schrieffer, J. R. & Su, W. P. Solitons in conducting polymers. *Rev. Mod. Phys.* **60**, 782–845 (1988).
15. Hernangomez-Perez, D., Gunasekaran, S., Venkataraman, L. & Evers, F. Solitonics with polyacetylenes. *Nano Lett.* **20**, 2615–2619 (2020).
16. Cheon, S., Kim, T., Lee, S. & Yeom, H. W. Chiral solitons in a coupled double Peierls chain. *Science* **350**, 182–185 (2015).
17. Oh, C. G., Han, S. H., Jeong, S. G., Kim, T. H. & Cheon, S. Particle-antiparticle duality and fractionalization of topological chiral solitons. *Sci. Rep.* **11**, 1013 (2021).
18. Song, S. K. & Yeom, H. W. Atomistic origin of metal versus charge-density-wave phase separation in indium atomic wires on Si(111). *Phys. Rev. B* **104**, 035420 (2021).
19. Kim, T., Cheon, S. & Yeom, H. W. Switching chiral solitons for algebraic operation of topological quaternary digits. *Nat. Phys.* **13**, 444–447 (2017).
20. Zhao, F., Cao, T. & Louie, S. G. Topological phases in graphene nanoribbons tuned by electric fields. *Phys. Rev. Lett.* **127**, 166401 (2021).
21. Gröning, O. et al. Engineering of robust topological quantum phases in graphene nanoribbons. *Nature* **560**, 209–213 (2018).
22. Cao, T., Zhao, F. & Louie, S. G. Topological phases in graphene nanoribbons: junction states, spin centers, and quantum spin chains. *Phys. Rev. Lett.* **119**, 76401 (2017).
23. He, Y., Wright, K., Kouachi, S. & Chien, C. Topology, edge states, and zero-energy states of ultracold atoms in one-dimensional optical superlattices with alternating on-site potentials or hopping coefficients. *Phys. Rev. A* **97**, 23618 (2018).
24. Chen, L. et al. Experimental observation of one-dimensional superradiance lattices in ultracold atoms. *Phys. Rev. Lett.* **120**, 193601 (2018).
25. Atala, M. et al. Direct measurement of the Zak phase in topological Bloch bands. *Nat. Phys.* **9**, 795–800 (2013).
26. Yang, Z. & Zhang, B. Acoustic type-II weyl nodes from stacking dimerized chains. *Phys. Rev. Lett.* **117**, 224301 (2016).
27. Xiao, M. et al. Geometric phase and band inversion in periodic acoustic systems. *Nat. Phys.* **11**, 240–244 (2015).
28. Yao, J. et al. Majorana-like end states in one-dimensional dimerized Kitaev topolectrical circuit. *N. J. Phys.* **24**, 043032 (2022).
29. Poshakinskiy, A. V., Poddubny, A. N. & Hafezi, M. Phase spectroscopy of topological invariants in photonic crystals. *Phys. Rev. A* **91**, 043830 (2015).
30. Verbin, M., Zilberberg, O., Kraus, Y. E., Lahini, Y. & Silberberg, Y. Observation of topological phase transitions in photonic quasicrystals. *Phys. Rev. Lett.* **110**, 076403 (2013).
31. Kraus, Y. E., Lahini, Y., Ringel, Z., Verbin, M. & Zilberberg, O. Topological states and adiabatic pumping in quasicrystals. *Phys. Rev. Lett.* **109**, 106402 (2012).
32. Park, J. W. et al. Creation and annihilation of mobile fractional solitons in atomic chains. *Nat. Nanotechnol.* **17**, 244–249 (2022).
33. Yue, S. et al. Observation of one-dimensional Dirac fermions in silicon nanoribbons. *Nano Lett.* **22**, 695–701 (2022).
34. Geng, D. et al. Observation of gapped Dirac cones in a two-dimensional Su-Schrieffer-Heeger lattice. *Nat. Commun.* **13**, 7000 (2022).
35. Wang, S. et al. On-surface synthesis and characterization of individual polyacetylene chains. *Nat. Chem.* **11**, 924–930 (2019).

36. Nurul, H. M., Shawulienu, K., Teemu, O., Drost, R. & Liljeroth, P. Tuneable topological domain wall states in engineered atomic chains. *npj Quantum Mater.* **5**, 17 (2020).
37. Jin, K. & Liu, F. 1D topological phases in transition-metal monochalcogenide nanowires. *Nanoscale* **12**, 14661–14667 (2020).
38. Zhou, M. et al. Epitaxial growth of large-gap quantum spin hall insulator on semiconductor surface. *Proc. Natl Acad. Sci. USA* **111**, 14378–14381 (2014).
39. Reis, F. et al. Bismuthene on a SiC substrate: a candidate for a high-temperature quantum spin hall material. *Science* **357**, 287–290 (2017).
40. Owen, J. H. G., Miki, K. & Bowler, D. R. Self-assembled nanowires on semiconductor surfaces. *J. Mater. Sci.* **41**, 4568–4603 (2006).
41. Miki, K., Bowler, D. R., Owen, J. H. G., Briggs, G. A. D. & Sakamoto, K. Atomically perfect bismuth lines on Si(001). *Phys. Rev. B* **59**, 14868 (1999).
42. Owen, J. H., Miki, K., Koh, H., Yeom, H. W. & Bowler, D. R. Stress relief as the driving force for self-assembled Bi nanolines. *Phys. Rev. Lett.* **88**, 226104 (2002).
43. Miwa, R. H., Macleod, J. M., Mclean, A. B. & Srivastava, G. P. The equilibrium geometry and electronic structure of Bi nanolines on clean and hydrogenated Si(001) surfaces. *Nanotechnology* **16**, 2427–2435 (2005).
44. Kirkham, C. J., Brazdova, V. & Bowler, D. R. Bi on the Si(001) surface. *Phys. Rev. B* **86**, 035328 (2012).
45. Longobardi, M. et al. Electronic coupling between Bi nanolines and the Si(001) substrate: an experimental and theoretical study. *Phys. Rev. B* **96**, 235421 (2017).
46. Kirkham, C. J., Longobardi, M., Köster, S. A., Renner, C. & Bowler, D. R. Subatomic electronic feature from dynamic motion of Si dimer defects in Bi nanolines on Si(001). *Phys. Rev. B* **96**, 075304 (2017).
47. Heyd, J. & Scuseria, G. E. Efficient hybrid density functional calculations in solids: assessment of the Heyd-Scuseria-Ernzerhof screened coulomb hybrid functional. *J. Chem. Phys.* **121**, 1187–1192 (2004).
48. Heyd, J., Peralta, J. E., Scuseria, G. E. & Martin, R. L. Energy band gaps and lattice parameters evaluated with the Heyd-Scuseria-Ernzerhof screened hybrid functional. *J. Chem. Phys.* **123**, 174101 (2005).
49. Zak, J. Berry's phase for energy bands in solids. *Phys. Rev. Lett.* **62**, 2747–2750 (1989).
50. Slot, M. R. et al. Experimental realization and characterization of an electronic Lieb lattice. *Nat. Phys.* **13**, 672–676 (2017).
51. Kempkes, S. N. et al. Robust zero-energy modes in an electronic higher-order topological insulator. *Nat. Mater.* **18**, 1292–1297 (2019).
52. Pavliček, N. et al. Synthesis and characterization of triangulene. *Nat. Nanotechnol.* **12**, 308–311 (2017).
53. Schindler, F., Tsirkin, S. S., Neupert, T., Andrei, B. B. & Wieder, B. J. Topological zero-dimensional defect and flux states in three-dimensional insulators. *Nat. Commun.* **13**, 5791 (2022).
54. Benalcazar, W. A., Li, T. & Hughes, T. L. Quantization of fractional corner charge in C*n*-symmetric higher-order topological crystalline insulators. *Phys. Rev. B* **99**, 245151 (2019).
55. Henkelman, G., Uberuaga, B. P. & Nsson, H. J. A climbing image nudged elastic band method for finding saddle points and minimum energy paths. *J. Chem. Phys.* **113**, 9901–9904 (2000).
56. Ye, C., Zhang, L. & Xue, H. Quantum transport signatures of non-trivial topological edge states in a ring-shaped Su-Schrieffer-Heeger double-chain system. *Chin. Phys. B* **31**, 27304–27634 (2022).
57. Zhou, M. et al. Strain-engineered surface transport in Si(001): complete isolation of the surface state via tensile strain. *Phys. Rev. Lett.* **111**, 246801 (2013).
58. Kiczynski, M. et al. Engineering topological states in atom-based semiconductor quantum dots. *Nature* **606**, 694–699 (2022).
59. Gurlu, O., Adam, O. A. O., Zandvliet, H. J. W. & Poelsema, B. Self-organized, one-dimensional Pt nanowires on Ge(001). *Appl. Phys. Lett.* **83**, 4610–4612 (2003).
60. Chan, T., Wang, C. Z., Lu, Z. & Ho, K. M. A first-principles study of group IV dimer chains on Si(100). *Phys. Rev. B* **72**, 45401–45405 (2005).
61. Kotlyar, V. G. et al. Surface reconstructions in Pb/Si(100) system: composition and atomic arrangement. *Surf. Sci.* **695**, 121574 (2020).
62. Mihalyuk, A. N., Chou, J. P., Eremeev, S. V., Zotov, A. V. & Saranin, A. A. One-dimensional Rashba states in Pb atomic chains on a semiconductor surface. *Phys. Rev. B* **102**, 035442 (2020).
63. Kresse, G. & Joubert, D. From ultrasoft pseudopotentials to the projector augmented-wave method. *Phys. Rev. B* **59**, 1758–1775 (1999).
64. Blochl, P. E. Projector augmented-rave method. *Phys. Rev. B* **50**, 17953 (1994).
65. Kresse, G. & Furthmüller, J. Efficiency of ab-initio total energy calculations for metals and semiconductors using a plane-wave basis set. *Comput. Mater. Sci.* **6**, 15–50 (1996).
66. Kresse, G. & Furthmuller, J. Efficient iterative schemes for ab initio total-energy calculations using a plane-wave basis set. *Phys. Rev. B* **54**, 11169–11186 (1996).
67. Perdew, J. P., Burke, K. & Ernzerhof, M. Generalized gradient approximation made simple. *Phys. Rev. Lett.* **77**, 3865–3968 (1996).
68. Wu, Q., Zhang, S., Song, H., Troyer, M. & Soluyanov, A. A. Wanniertools: an open-source software package for novel topological materials. *Comput. Phys. Commun.* **224**, 405–416 (2018).
69. Pizzi, G. et al. Wannier90 as a community code: new features and applications. *J. Phys. Condes. Matter* **32**, 165902 (2020).
70. Zhi, G. X., Xu, C. C., Wu, S. Q., Ning, F. L. & Cao, C. Wannsymm: a symmetry analysis code for wannier orbitals. *Comput. Phys. Commun.* **271**, 108196 (2022).

Acknowledgements

This work is supported by the Natural Science Foundation of Zhejiang Province (Grant No. LZ22A040004), the National Key R&D Program of China (Grant No. 2022YFF0708800), the National Natural Science Foundation of China (Grant No. 11674042), and the Thousand Youth Talents Program of China. We also acknowledge the support from the Center for High-Performance Computing of Beihang University (BHHPC) and the High-Performance Supercomputing Center of International Innovation Institute, Beihang University.

Author contributions

B.S. performed the theoretical calculations. B.S., G.Z., C.H. and M.Z. analyzed the results of simulations. B.S. and M.Z. co-wrote the manuscript. All authors contributed to the discussion and reviewed the manuscript. M.Z. conceived the idea and supervised the project.

Competing interests

The authors declare no competing interests.

Additional information

Supplementary information The online version contains supplementary material available at https://doi.org/10.1038/s41535-024-00637-3.

Correspondence and requests for materials should be addressed to Miao Zhou.